
PhiP-G: Physics-Guided Text-to-3D Compositional Scene Generation

Qixuan Li^{1,2} Chao Wang^{1,2†} Zongjin He^{1,2} Yan Peng^{1,2}

Abstract

Text-to-3D asset generation has achieved significant optimization under the supervision of 2D diffusion priors. However, when dealing with compositional scenes, existing methods encounter several challenges: 1). failure to ensure that composite scene layouts comply with physical laws; 2). difficulty in accurately capturing the assets and relationships described in complex scene descriptions; 3). limited autonomous asset generation capabilities among layout approaches leveraging large language models (LLMs). To avoid these compromises, we propose a novel framework for compositional scene generation, PhiP-G, which seamlessly integrates generation techniques with layout guidance based on a world model. Leveraging LLM-based agents, PhiP-G analyzes the complex scene description to generate a scene graph, and integrating a multimodal 2D generation agent and a 3D Gaussian generation method for targeted assets creation. For the stage of layout, PhiP-G employs a physical pool with adhesion capabilities and a visual supervision agent, forming a world model for layout prediction and planning. Extensive experiments demonstrate that PhiP-G significantly enhances the generation quality and physical rationality of the compositional scenes. Notably, PhiP-G attains state-of-the-art (SOTA) performance in CLIP scores, achieves parity with the leading methods in generation quality as measured by the T³Bench, and improves efficiency by 24x.

1. Introduction

Text-to-3D models (Zhu et al., 2024; Poole et al., 2023; Lin et al., 2023; Liu et al., 2024) are systems that convert natural language descriptions into 3D assets by integrating

¹School of Future Technology, Shanghai University, Shanghai, 200444, China. ²Institute of Artificial Intelligence, Shanghai University, Shanghai, 200444, China. Correspondence to: Chao Wang <cwang@shu.edu.cn>.

Under review.

techniques like 2D-to-3D conversion, neural implicit representation, and 3D mesh generation, leveraging deep learning for cross-modal and diverse 3D content creation. There is a growing demand for high-quality 3D assets, particularly for training scenarios in autonomous driving (Mittal, 2020) and robotic navigation (Bermejo et al., 2021). In contrast, 3D content creation, especially for complex scenes, often requires substantial time and effort from domain experts, resulting in constrained production capacity. The advent of text-to-3D technologies offers a novel solution to this challenge, empowering non-expert users to create 3D assets through natural language. However, existing 3D generation methods typically prioritize improving the quality of individual asset, while paying insufficient attention to tasks like compositional scene generation.

Compositional scene generation refers to the process of generating a finite number of 3D assets based on scene descriptions and arranging them in a physically plausible layout. Current mainstream text-to-3D models generally lack an understanding of complex semantics and guidance for the layout of scene-level 3D assets. As a result, generating the compositional 3D scene involving multiple objects frequently gives rise to disorganized layouts and inadequate physical consistency. (i.e., **issue 1**). Concurrently, a recent trend (Bai et al., 2024; Cohen-Bar et al., 2023; Po & Wetstein, 2023) involves manually designed layouts to impose geometric constraints, capturing relationships among multiple objects in the scene, and using implicit neural radiance fields (NeRF) (Mildenhall et al., 2020) for generation. However, this approach struggles to meet all constraints in the layout, leading to blurry textures and geometric distortions (i.e., **issue 2**). In contrast, some recent 3D scene generation methods employ LLMs as agents to analyze textual descriptions and leverage the reasoning capabilities of LLMs for layout guidance (Kumaran et al., 2023; Yang et al., 2024). Nevertheless, these models often focus only on 3D asset layouts, requiring assets to be sourced from existing 3D asset libraries. Such limitations inherently constrains their 3D asset generation capabilities, significantly reducing the flexibility of the generation model (i.e., **issue 3**). From the above issues, 3D compositional scene generation emerges as a task that extends beyond merely stacking assets. This task requires models with exceptional single-asset generation capabilities, advanced semantic understanding, and physics-

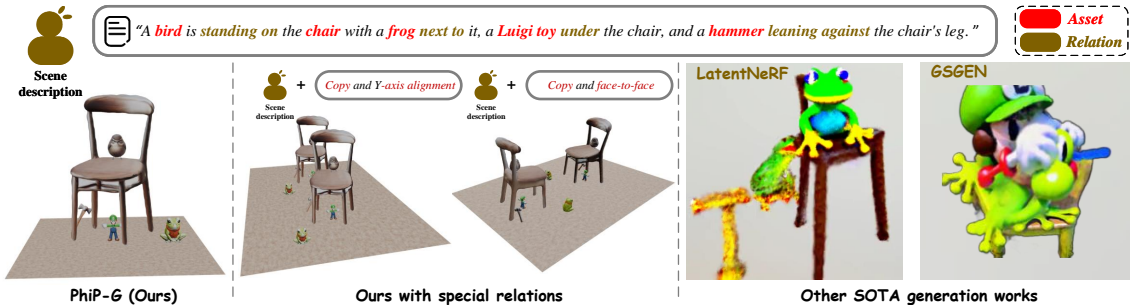


Figure 1. **PhiP-G** is dedicated to understanding complex scene descriptions and generating high-quality 3D compositional scenes while supporting the generation of special scene relationships. Compared with existing generation methods, our method demonstrates excellent physical consistency and the ability to handle special environmental relationships.

based layout guidance. The absence of any component can result in catastrophic quality in compositional scene. As shown in the right panel of Figure 1, traditional methods lacking physical layout guidance and complex semantic understanding lead to chaotic results.

In this paper, we propose a framework named **PhiP-G** (Physics-Guided Text-to-3D Compositional Scene Generation) for generating high-quality 3D scenes from complex natural language inputs. In **PhiP-G**, we integrate generative models with LLM-based agents for 3D asset generation. And then we utilize the predictive and planning capabilities of the world model (Ha & Schmidhuber, 2018; Micheli et al., 2023; Zhang et al., 2021) during the layout phase to construct high-quality 3D scenes that comply with physical laws and align with textual descriptions, without additional training. Specifically, we employ LLM-based agents to perform semantic parsing and relationship extraction on complex textual inputs, generating a scene graph to avoid manual layout by the user (addressing **issue 2**).

Simultaneously, we combine a DALL-E 3-based 2D image generation agent with the 3D Gaussian splatting (3DGS) (Kerbl et al., 2023) generation model DreamGaussian (Tang et al., 2023), incorporating a CLIP-based (Radford et al., 2021) score filtering mechanism and a 2D image retrieval library to form the 3D asset generation module. The module enables flexible generation of high-quality assets based on the decomposed scene graph (addressing **issue 3**).

We use Blender as the foundational platform for layout design, introducing a physical pool with a *physical magnet* and a relationship-matching agent for coarse compositional scene layout. A visual supervision agent evaluates coarse layout and provides iterative fine-tuning guidance. These two stages of layout guidance form the world model, demonstrating excellent performance in semantic consistency with complex textual inputs and adherence to physical laws (addressing **issue 1**). Extensive experiments demonstrate that **PhiP-G** achieve free, flexible, and physically consistent high-quality 3D compositional scene generation without

requiring additional training.

Our **contributions** can be summarized as follows:

- We propose a framework **PhiP-G**, based on 3DGS for text-to-3D generation and world model-based scene layout, which enables the rapid generation of the high-quality, continuous, and physically consistent 3D compositional scene from textual prompts.
- **PhiP-G** enhances the understanding of complex scene descriptions through a multi-agent text preprocessing mechanism, incorporates a physical pool with a physical magnet, and leverages world model attribute prediction to improve the physical coherence of compositional scene layout guidance.
- In extensive 3D composite scene generation experiments, **PhiP-G** achieves SOTA on the semantic consistency metric CLIP. Particularly, on the T³Bench metric, it matches SOTA in overall performance while improving generation efficiency by 24 times.

2. Related Work

3DGS for text-to-scene generation. Traditional text-to-3D methods primarily rely on generative approaches based on adversarial networks or variational autoencoders (Zhao et al., 2022; Ko et al., 2023; Ferreira et al., 2022; Kosiorok et al., 2021; Eguchi et al., 2022; Petrovich et al., 2021), utilizing 2D images or textual descriptions to infer and generate complex 3D shapes, which are often computationally expensive and slow to produce. The recently popular 3DGS (Kerbl et al., 2023) demonstrates a method for representing 3D spaces by optimizing 3D Gaussian spheres, enabling fast rendering and making it popular in 3D scene reconstruction. (Chung et al., 2023) generates 3D scenes through image inpainting with stable diffusion (Rombach et al., 2021), using reference images or text to expand different viewpoints. GALA3D (Zhou et al., 2024) utilizes object-level text-to-3D modeling, and MVDream (Shi et al., 2023) generates

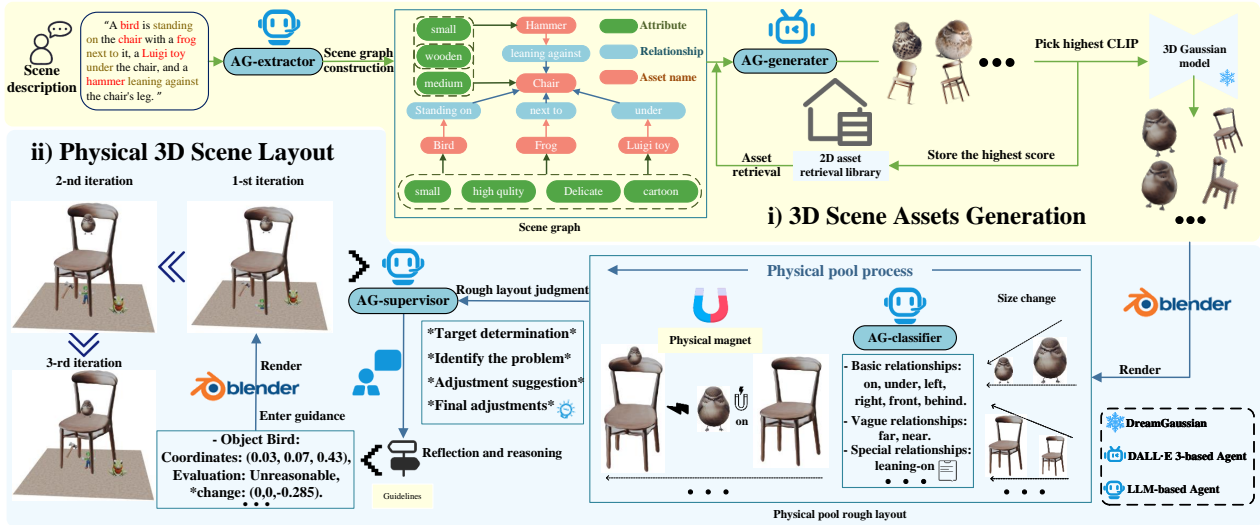


Figure 2. **Overview of PhiP-G.** Given a complex scene description, PhiP-G employs an LLM-based agent to perform text analysis and construct a scene graph. Graph-based 3D asset generation is carried out using a 2D generation agent and the 3D Gaussian model, where the 2D asset with the highest CLIP score is stored in the 2D retrieval library for future use. Subsequently, Blender serves as the foundational environment, where a world model consisting of the physical pool and a visual supervision agent enables coarse layout and iterative refinement. PhiP-G ensures improved semantic consistency and physical coherence in the generated scene.

realistic objects, combining them using scene-level diffusion models. Text-to-scene generation methods based on 3DGS excel in specific tasks but struggle with consistency and stability in complex, detail-rich scenes. Moreover, their training demands substantial computational resources. Our approach integrates 3DGS with LLM-based scene layout, utilizing 3DGS for individual asset generation to enhance speed and stability while ensuring broad compatibility with most 3DGS methods without requiring additional training.

Multimodal LLM agents for scene generation. With the advancement of multimodal LLMs, models equipped with visual perception capabilities, such as GPT-V (OpenAI, 2023), have become increasingly sophisticated. Consequently, there is a growing interest in integrating multimodal LLMs into 3D scene generation tasks. For instance, Holodeck (Yang et al., 2024) employs a multi-stage process to transform initial 3D scene layouts derived from text into realistic environments. The process uses ChatGPT-4 (OpenAI, 2023) for spatial reasoning, layout generation, material selection, and object arrangement, optimizing spatial relationships to achieve realistic 3D interactions. Similarly, SceneCraft (Kumaran et al., 2023) utilizes a modular architecture with LLMs to iteratively convert textual descriptions into 3D spatial layouts, object selection, and attribute settings, enabling interactive 3D world creation and code generation from natural language instructions. However, most LLM-based scene generation methods rely on LLMs for reasoning, code generation, and asset retrieval, but are limited by their inability to independently create 3D assets and their dependence on pre-existing libraries. In contrast, our

approach fully leverages the advanced multimodal capabilities of LLMs and integrates a 3DGS model, allowing for the free generation of target 3D assets from scene descriptions.

3. Method

3.1. Overview

As illustrated in Figure 2, our overall framework consists of two main components: 1). 3D assets generation, and 2). physical 3D scene layout. For the first component, a keyword extraction agent infers the scene graph and relationships from a complex scene description T , followed by the generation of 3D assets using a 2D image generation agent and a 3D Gaussian generation model (Section 3.2). For the second component, the framework incorporates a designed physical pool with a relationship classification agent and an iterative fine-tuning visual supervision agent as part of the world model, enabling a two-stage compositional scene layout (Section 3.3).

3.2. Generation of High-Quality 3D Scene Assets

This section mainly introduces the process of generating 3D scene objects from scene descriptions. First, we explain how the scene descriptions are processed. Then, we describe the use of the treated text in generating 3D scene assets.

Scene description processing. When our brain receives a description of a complex scene, we instinctively think about the objects in the scene and their sizes and relationships. Analogously, when constructing a 3D scene from a

description, a “brain” is required to process it. Therefore, we design a keyword extraction agent, `AG-extractor`, which uses the Chain of Thought (CoT) reasoning (Wei et al., 2023) method to decompose complex scene descriptions and generate a scene graph $G(\cdot)$, as shown in Figure 2. First, for the scene description statement T , we use the agent to decompose and extract all assets in the scene $A = \{a_i \mid i \in [1, \dots, k]\}$, where k is the total number of scene assets. The descriptions are then enriched and refined to obtain asset text descriptions more suitable for 2D generation, represented as $\hat{A} = \{\hat{a}_i \mid i \in [1, \dots, k]\}$. Next, the keyword extraction agent evaluates the size of each extracted asset a_i and generates an asset size classification $Z = \{z_i \mid i \in [1, \dots, k]\}$. We categorize asset sizes into three types: large, medium, and small.

After reasoning the size of each asset, keyword extraction agent performs basic relationship reasoning based on each asset’s name a_i , size z_i , and their relationships within the scene description. To avoid the extensive spatial relationship training required in previous layout methods, we sort the assets according to their extraction order. The agent selects the second asset as the core asset and infers the relative spatial relationships between each asset and the core asset. These relationships are described as $R = \{r_i \mid i \in [1, \dots, k]\}$. Since the core asset corresponds to $i = 2$, its relationship r_2 is set to `None`. Such method allows for initial positioning and incremental scene layout based solely on the object order and their relationships to the core asset. As a result, no additional training is needed. After determining the basic relationships, we infer the special relationships for the overall scene, such as duplication requirements and alignment strategies. The special relationships are denoted as $S \in \{s_1, s_2, s_3\}$, where, s_1 , s_2 , and s_3 represent the x -axis, y -axis, and face-to-face alignment, respectively. At this point, we successfully obtain the scene graph $G(T) = (S, A, Z, R)$ for the complex scene description. The entire formal expression of the extractor can be shown as $\text{AG-extractor}(T) \rightarrow (S, A, Z, R) = G(T)$. where, A , Z , and R respectively represent all the extracted assets in the scene, their corresponding sizes, and their relationships with the core assets.

3D scene assets generation. For the 3D scene asset generation part, we use the enriched asset descriptions \hat{A} as generation prompts. To ensure both generation quality and speed, we divide the 3D asset generation into two parts: 1). using a 2D generation agent to convert the asset descriptions into 2D images, and 2). rapidly generating 3D assets from the 2D images through a Gaussian generation model.

For the first part, we design a 2D generation agent, `AG-generator`, which is based on DALL-E 3 to generate 2D images $I_{2D} = \{i_{2D}^j \mid j \in [1, \dots, k]\}$ from textual descriptions \hat{A} . Due to the excessively rich training

samples of DALL-E 3, the 2D generation process often produces abundant backgrounds and elements outside the descriptions, which can adversely affect the subsequent 3D generation. Therefore, we further use prompt engineering on `AG-generator` to constrain the generation requirements, including specifications for backgrounds, shadows, and material textures of objects. To further ensure semantic consistency between the 2D-generated images and asset descriptions, we adopt a looped generation process to produce multiple images (typically five).

And then, we calculate their CLIP scores relative to the asset descriptions and select the image $i_{2D\text{Max}}^j$ with the highest text similarity for subsequent 3D generation. The above processing steps ensure the quality and semantic consistency of the generated 2D images, which is also beneficial for subsequent 3D asset generation. The overall formal expression of the 2D generation agent is $\text{AG-generator}(\hat{A}) \rightarrow (i_{2D\text{Max}}^1, \dots, i_{2D\text{Max}}^k)$. In addition to directly generating images from text, we have established a 2D image retrieval library. When the required asset is present in the retrieval library, the image is invoked directly, bypassing the text-to-2D process of the `LLM-generator`. If the asset is not found, the image with the highest CLIP score $i_{2D\text{Max}}^j$, is assigned a name based on the asset and stored in the retrieval library. Additionally, the retrieval library enables users to manually name and store specific 2D images, enhancing stability during multiple generations, improving generation efficiency, and eliminating semantic ambiguity related to the need for specific assets in the scene.

For the second part, considering the need for fast 3D asset generation while ensuring quality, we choose the 3D Gaussian generation model. For each scene asset, the 2D image with the highest CLIP score undergoes background removal and repositioning to ensure a clean background and precise object centering. Processed images serve as input to the Gaussian generation model, enabling rapid 3D assets generation. Once the 3D Gaussian assets are obtained, we convert them into the glb format $I_{3D} = \{i_{3D}^j \mid j \in [1, \dots, k]\}$. Compared to the original 3D Gaussian data, glb format is more convenient for downstream tasks and facilitates our subsequent scene layout process. By extracting and transforming assets from scene descriptions into 3D, the scene layout no longer relies on pre-existing 3D data asset libraries, significantly improving the flexibility of the overall compositional scene generation task.

3.3. Two-Stage Compositional 3D Scene Layout

This section primarily describes the two-stage compositional scene layout process based on the world model. In the first stage, we implement an initial scene layout through the design of simple and effective physical pool. In the second stage, we design a scene layout supervision agent

that optimizes the scene layout through a feedback loop with supervised learning. The two-stage process together forms the world model framework, enabling the prediction and planning of scene layouts based on existing information and 3D assets.

Preliminary layout design. In the first stage of the scene layout, based on the scene graph $G(T)$ and the generated 3D scene assets, we designed a physical pool to perform the preliminary layout. Within the physical pool, we define a relational database with rich relationships, classifying basic physical relationships in the real world. And then, we introduce a classification agent called `AG-classifier` to match the inter-asset relationships with the relational database. The agent identifies these relationships as the standard relationships between 3D assets denoted as $\hat{R} = \{\hat{r}_i \mid i \in [1 \dots k]\}$, as shown in $\text{AG-classifier}(R) \rightarrow (\hat{r}_1, \dots, \hat{r}_k)$. This approach standardizes the types of relationships, clarifying abstract relationship descriptions, which facilitates unified management and invocation of spatial relationships. Due to the fact that the assets generated by the 3D Gaussian generation model are of nearly the same size, we need to uniformly scale the assets based on their inferred sizes so that their dimensions conform to real-world physical laws. Next, we perform coarse bounding box extraction, which involves obtaining the local bounding boxes of the objects and mapping them to the world coordinate system. We displace the 3D assets according to the standardized relationship \hat{R} , such that the bounding boxes are tangential in the corresponding standardized manner. For example, the relationship “on” means that the bottom of one asset is tangential to the top of another. The above process completes the rapid displacement and preliminary arrangement of the 3D scene assets.

Simple bounding box intersection alone is insufficient. For instance, in the scene where “a bicycle leans against a tree”, predefined bounding boxes may create gaps between objects, failing to accurately capture physical interaction. To address this, the *physical magnet* is designed to apply vector approximation to the nearest points of two assets, enabling the front asset to “adhere” to the back asset, similar to the behavior of a magnet. Specifically, it functions as follows: we first utilize Alpha-shape to reconstruct the boundary shape of the 3D assets, obtaining the detailed contour of the asset. To reduce excessively dense and meaningless vertices on the detailed contour, we leverage Blender’s merge vertex function and the *Decimate* modifier to simplify the vertices and mesh, thus lightweighting the detailed contour representation. Then, we select pairs of 3D asset objects that have mutual relationships, iterating through the vertices \mathcal{V} of their detailed contours to calculate the distances and directional vectors of their nearest vertices. By using a contact distance threshold d_{thresh} , we determine whether there is contact between these two assets. If no contact exists,

we displace the former asset according to the nearest vertex distance and direction vector.

The *physical magnet* effectively eliminates the empty spaces caused by simple bounding box tangency that violate physical laws, enabling touch-based contact between two assets without requiring training. Under the combined influence of bounding box tangency constraints in asset relationships and the *physical magnet*, a rapid preliminary scene layout is generated, which partially adheres to physical laws. However, this preliminary layout may be insufficient for more complex scenes. The *physical magnet* can lead to violations of physical laws, such as causing a bird to be attracted to the back of the chair when describing a scenario exemplified by “a bird standing on a chair”. The formal expression of the entire *physical magnet* is given as:

$$\begin{aligned} \mathcal{V}_{\text{simplified}} &= \text{Decimate}(\mathcal{V}_{\text{orig}}), \quad |\mathcal{V}_{\text{simplified}}| < |\mathcal{V}_{\text{orig}}|, \\ d(v_1, v_2) &= \min_{v_2 \in \mathcal{V}_2} \|v_1 - v_2\|, \quad \vec{d}(v_1, v_2) = v_2 - v_1, \\ v_1 + \lambda \cdot \vec{d}(v_1, v_2) &\rightarrow v_1^{\text{new}} \quad \text{if } d(v_1, v_2) > d_{\text{thresh}}. \quad (1) \end{aligned}$$

where, $\mathcal{V}_{\text{orig}}$ and $\mathcal{V}_{\text{simplified}}$ represent the original and simplified vertex sets, respectively. v_1 and v_2 denote the current object’s vertex and the nearest vertex of the target object. d_{thresh} defines the vertex contact threshold, λ scales the vertex displacement, and v_1^{new} represents the updated vertex position for guiding asset displacement.

Feedback loop for layout optimization. To further optimize the scene layout, we designed a visual supervision loop for iterative improvement. By utilizing a scene supervisor agent with visual capabilities, the `AG-supervisor`, the preliminary layout is evaluated from the perspective of physical commonsense, and guidance is provided for layouts that do not conform to commonsense. To enable the supervisor agent to better understand the required reasoning process and reduce ineffective reasoning, we introduce a reflective process, i.e., reverse reasoning. In the reverse reasoning process, the final target result is first provided, which is that all objects should be correctly placed. Then, we provide examples and detailed adjustment suggestions, including reasoning for layout adjustments and calculations of displacement distances and directions for the assets. Finally, the framework validates the adjustments to assess the rationality of the move. Such reflection process enhances the adaptability and decision-making quality of the world model in dynamic layout tasks. In the t -th iteration, we place cameras along the x -axis, y -axis, and z -axis in the scene layout, and direct them towards the origin to capture simple scene layout reference images from three perspectives, denoted as $P_t = \{I_X, I_Y, I_Z\}$. We use the three-perspective reference images P_t , the original scene description T , and the scene graph $G(T)$ as reasoning inputs. The supervisor agent evaluates the rationality of the asset layout and its relation-

Table 1. **Quantitative analysis of text-to-3D scene layout relies on the CLIP metric.** The advanced methods involved in the comparison are categorized based on model types. ● SCENE 1, ○ SCENE 2, ● SCENE 3, and ● SCENE 4 represent scenes generated using different numbers of assets, with the 3D asset counts being respectively 3, 4, 6, and 8.

METHODS	MODEL TYPE	● SCENE 1	○ SCENE 2	● SCENE 3	● SCENE 4
LATENTNERF (METZER ET AL., 2022)	NeRF	29.68	24.96	27.87	22.59
MVDREAM (SHI ET AL., 2023)	NeRF	30.72	25.04	28.59	25.82
SJC (WANG ET AL., 2022)	VOXEL GRID	27.05	26.10	24.45	25.62
DREAMFUSION (POOLE ET AL., 2023)	3DGS	27.33	24.15	27.39	21.01
MAGIC3D (LIN ET AL., 2023)	3DGS	30.46	23.06	27.89	26.83
DREAMGAUSSIAN (TANG ET AL., 2023)	3DGS	25.37	18.35	25.19	23.15
GSGEN (CHEN ET AL., 2024)	3DGS	30.28	27.40	28.41	30.30
PHIP-G (OURS)	3DGS + AGENTS	33.17	36.80	33.04	34.24

ships based on these inputs. The evaluation uses an exact matching mechanism to project complex natural language information into a two-dimensional discrete binary reward score, labeling assets as either “positive” or “negative”. For assets labeled as “negative”, the AG-supervisor will further provide layout guidance, i.e., based on the asset attributes and the scene, it will offer optimal scene layout suggestions L_t . The formal expression of the supervisor is shown as $\text{AG-supervisor}(P_t, T, G(T)) \rightarrow L_t$. After the layout optimization is complete, we introduce a scoring function S to evaluate the layout quality after each optimization guidance, which is used to comprehensively measure the rationality of the layout and the cost of adjustments. The definition is as follows:

$$S = 1 - \frac{1}{N} \sum_{i \in I_{3D}} \left(\alpha \cdot \text{Violation}_i + \beta \cdot \frac{|\Delta C_i|}{\Delta_{\max}} \right) \quad (2)$$

Here, N is the total number of 3D assets, and Violation_i represents the physical violation degree of asset i . ΔC_i denotes the adjustment displacement of asset i , while Δ_{\max} , the maximum allowable adjustment distance, is defined as $\Delta_{\max} = 0.5$. The coefficients α and β balance the impact of violation degree and adjustment displacement on scoring.

When the layout score S_t of the t -th iteration is lower than the previous score S_{t-1} , the current iteration’s layout guidance is discarded, and rationality planning is redone. Conversely, if S_t exceeds the rationality threshold, the layout iteration concludes as reasonable. Otherwise, the layout optimization process repeats until the rationality check is satisfied. Thus, the looped supervision optimization part for the preliminary layout concludes. In the two-stage layout of complex 3D scenes, we fully utilize the predictive planning capabilities of the world model, composed of the physical pool and agents, so that the layout itself does not require training. Compared to traditional layout tasks, this approach saves significant time and computational costs, while yielding satisfactory results.

To enhance the realism of the scene generation, after the layout optimization is completed, we use Blender’s built-in

particle system to simulate realistic ground surfaces. Three types of realistic ground are simulated: grass, wood, and sand. Meanwhile, we invoke the agent AG-extractor to analyze the scene and determine which type of ground is most suitable. Then, the agent will iterate through the bottom faces of all objects’ bounding boxes, identifying the lowest face, and generate the simulated ground at the position where it is tangent to this face.

4. Experiments

4.1. Quantitative Comparison

Quantitative analysis uses the CLIP metric. In Table 1, we use the text-image similarity metric CLIP for qualitative evaluation, analyzing the consistency and quality between text descriptions and 3D scenes. We also compare the performance of our method with current SOTA methods on the task of text-to-3D complex scene construction. To improve the reliability of the benchmark, we consider various 3D reconstruction and representation techniques when selecting advanced methods, including NeRF-driven approaches, voxel-based representation methods, and techniques based on 3D geometric structures. Our approach integrates agents based on the world model while utilizing 3D GS for generation. For a comprehensive demonstration of each model’s generation capabilities across diverse 3D scenes, we test scene prompts containing 3, 4, 6, and 8 assets. Ultimately, ours achieves higher CLIP scores than other generation models in the text-to-3D compositional scene generation and layout task, demonstrating better semantic consistency between text and scenes.

Quantitative analysis uses the T³Bench metric. To further evaluate the generation quality and semantic consistency of ours, we used the evaluation metrics provided by T³Bench (He et al., 2023), as shown in Table 2. The results of other methods in the table are derived from T³Bench, a comprehensive text-to-3D benchmark specifically designed for evaluating the quality of 3D generation. Its quality metrics combine multi-view text-image scoring and regional convo-

Table 2. Quantitative analysis of text-to-3D scene layout relies on the T³Bench metric. The **Quality** metric evaluates quality and view inconsistency. The **Alignment** metric measures the consistency between text and 3D scene. The **Average** is calculated as the average of the quality metric and the alignment metric, reflecting the overall performance of the model.

METHODS	RUNNING TIME ↓	QUALITY ↑	ALIGNMENT ↑	AVERAGE ↑
DREAMFUSION (POOLE ET AL., 2023)	30MINS	17.3	14.8	16.1
MAGIC3D (LIN ET AL., 2023)	40MINS	26.6	24.8	25.7
LATENTNERF (METZER ET AL., 2022)	65MINS	21.7	19.5	20.6
FANTASIA3D (CHEN ET AL., 2023)	45MINS	22.7	14.3	18.5
SJC (WANG ET AL., 2022)	25MINS	17.7	5.8	11.7
PROLIFICDREAMER (WANG ET AL., 2023)	240MINS	45.7	25.8	35.8
MVDREAM (SHI ET AL., 2023)	30MINS	39.0	28.5	33.8
DREAMGAUSSIAN (TANG ET AL., 2023)	7MINS	12.3	9.5	10.9
GEODREAM (MA ET AL., 2023)	400MINS	34.3	16.5	25.4
RICHDREAMER (QIU ET AL., 2024)	70MINS	34.8	22.0	28.4
PHIP-G (OURS)	10MINS	42.3	29.8	36.4

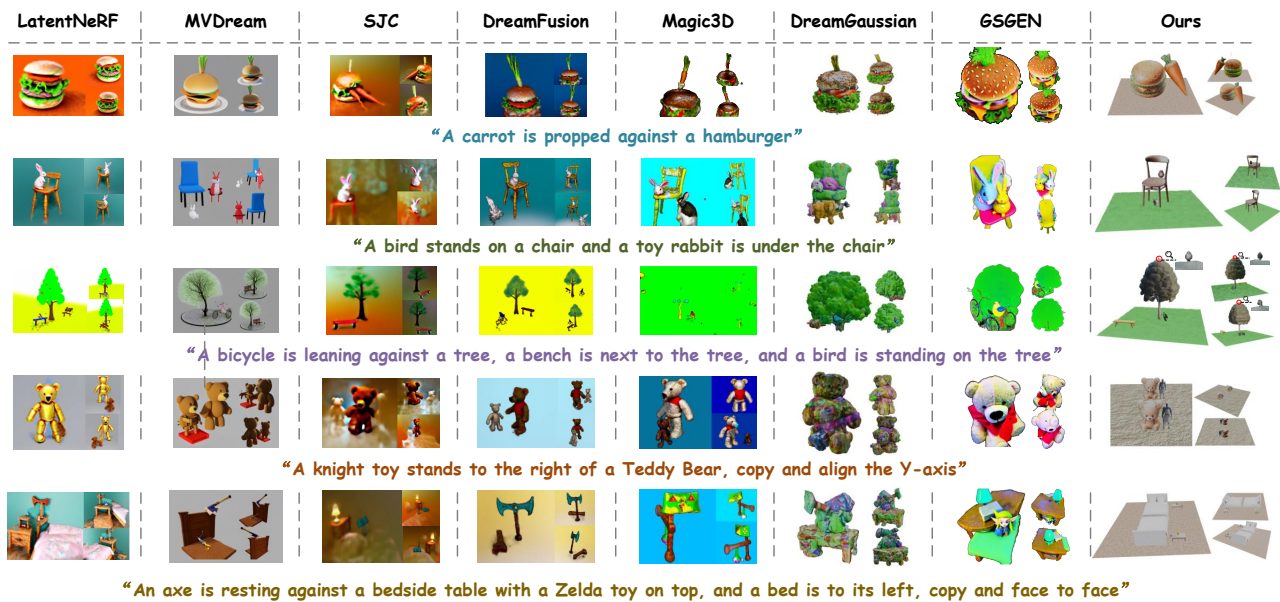


Figure 3. Qualitative analysis of text-to-3D scene. Our method ensures consistency between textual descriptions and generated 3D scenes, while maintaining physical laws and handling special layout requirements.

lution to detect quality and view inconsistency, while alignment metrics leverage multi-view caption generation and GPT-4 evaluation to measure the consistency between text and 3D content. The evaluation reveals our method achieves the best average performance, with slightly lower quality compared to ProlificDreamer, but a generation time reduced to just one twenty-fourth. The above results fully demonstrates that PhiP-G ensures high scene generation quality while maintaining fast generation speed. Additionally, by utilizing the world model composed of agents, semantic alignment is effectively guaranteed.

4.2. Qualitative Comparison

In the qualitative comparison section, we evaluate our method against SOTA generation models for 3D compo-

sitional scene generation performance. To comprehensively demonstrate the quality of the generated scenes, visual displays from the front, back, and side views for each model. As shown in the Figure 3, our approach demonstrates superior scene generation quality and semantic consistency.

For scenes with more complex textual descriptions, other methods show varying degrees of semantic understanding deviations and missing described assets. Furthermore, when textual descriptions include physical and spatial relationships between assets, others often produce disorganized and misaligned results. In contrast, our approach accurately captures the inter-asset relationships described in the text while maintaining layout rationality and physical consistency in the scene. For specific scene generation requirements, such as “Copy and face to face”, our approach demonstrates clear comprehension and effectively implements these require-

Table 3. User study on the results of scene generation. We conduct a user study to compare our method with the latest related works. Four metrics are selected to evaluate scene quality: text fidelity, scene quality, aesthetics, and physical rationality (PR), where higher scores (on a scale of 0-5) indicate better performance.

METHODS	TEXT FIDELITY	SCENE QUALITY	AESTHETIC	PR
MVDREAM (SHI ET AL., 2023)	3.41	3.12	2.84	3.23
SJC (WANG ET AL., 2022)	3.36	2.99	2.52	2.64
DREAMGAUSSIAN (TANG ET AL., 2023)	2.15	2.61	2.09	2.73
GSGEN (CHEN ET AL., 2024)	2.71	3.27	2.12	3.12
PHIP-G (OURS)	4.55	4.32	4.87	4.95

ments in a logical manner.

Table 4. Scene layout key step ablation. The term “w/o LLM-s” refers to ablating AG-supervisor. “w/o LLM-s & PM” refers to ablating both AG-supervisor and the *physical magnet*. “w/o physical pool” refers to ablating the physical pool, while “w/o All” refers to ablating all the aforementioned components.

METHODS	TIME ↓	CILP ↑
PHIP-G (OURS)	10MINS	35.63
w/o LLM-s	9MINS	31.93
w/o LLM-s & PM	8MINS	29.55
w/o PHYSICAL POOL	25MINS	30.14
w/o ALL	7MINS	23.25

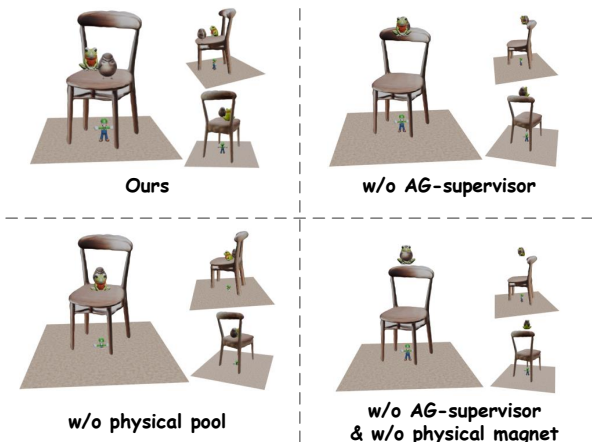


Figure 4. Visualization depicting the ablation of key steps. This ablation experiment visually demonstrates the effectiveness and necessity of each layout module we design.

4.3. Ablation Study

In Table 4, we conduct ablation experiments on the key steps of scene layout. Specifically, we perform ablations in four aspects: 1). The intelligent agent AG-supervisor as the layout supervisor. 2). Both AG-supervisor and the *physical magnet*. 3). The entire physical pool process. 4). Removing all three components above simultaneously. The comparison results indicate that our overall layout process effectively balances scene generation time and quality. The absence of AG-supervisor and the *physical magnet* leads to a decrease in generation quality. Moreover,

removing the physical pool-based rapid coarse layout significantly increases the optimization iterations required by AG-supervisor, resulting in a substantial increase in fine-tuning time. Figure 4 in presents a visual ablation experiment on key steps. The results show that removing the physical pool forces the supervising agent to handle fine-grained layouts directly, resulting in misaligned assets. When the AG-supervisor is removed, the lack of agent supervision causes coarse layouts through the physical pool without fine-tuning, leading to assets being pulled toward the chair back due to the *physical magnet*.

4.4. User Study

To comprehensively evaluate the scene generation quality of our method, we design a user study, as shown in the table 3. In this experiment, we introduce four evaluation metrics: text fidelity, scene quality, aesthetics, and physical rationality. We invite 73 volunteers to evaluate the scenes generated by our method and other popular models based on these metrics, assigning scores from 0 to 5. Higher scores indicate greater approval of the corresponding aspect of the generated results. From the table, it can be observed that our method performs the best across all metrics, demonstrating that it is more favored by users in scene generation and holds greater potential for further applications. The detailed setup of the overall aforementioned experiments can be found in Appendix A.1.

5. Conclusion

In this paper, we present PhiP-G, a novel text-to-3D compositional scene generation framework that combines advanced 3D Gaussian generation techniques with world model-based layout guidance. The framework excels in generating 3D scenes with strong textual consistency and physical coherence. Extensive experiments validate that PhiP-G outperforms existing methods in compositional scene generation, demonstrating superior semantic understanding and multi-object layout capabilities. Our future work will focus on: 1). Incorporating higher-quality 3D generation models into the framework as the 3D generation module; 2). Enhancing the integration of world models for more advanced complex scene generation.

References

- Bai, H., Lyu, Y., Jiang, L., Li, S., Lu, H., Lin, X., and Wang, L. Comperf: Text-guided multi-object compositional nerf with editable 3d scene layout, 2024. URL <https://arxiv.org/abs/2303.13843>.
- Bermejo, C., Lee, L.-H., Chojecki, P., Przewozny, D., and Hui, P. Exploring button designs for mid-air interaction in virtual reality: A hexa-metric evaluation of key representations and multi-modal cues. *Proceedings of the ACM on Human-Computer Interaction*, 5(EICS):194:1–194:26, 2021. doi: 10.1145/3457141.
- Chen, R., Chen, Y., Jiao, N., and Jia, K. Fantasia3d: Disentangling geometry and appearance for high-quality text-to-3d content creation. In *Proceedings of the IEEE/CVF International Conference on Computer Vision (ICCV)*, pp. 22246–22256, October 2023.
- Chen, Z., Wang, F., Wang, Y., and Liu, H. Text-to-3d using gaussian splatting, 2024. URL <https://arxiv.org/abs/2309.16585>.
- Chung, J., Lee, S., Nam, H., Lee, J., and Lee, K. M. Lucidreamer: Domain-free generation of 3d gaussian splatting scenes. *arXiv preprint arXiv:2311.13384*, 2023.
- Cohen-Bar, D., Richardson, E., Metzger, G., Giryes, R., and Cohen-Or, D. Set-the-scene: Global-local training for generating controllable nerf scenes, 2023. URL <https://arxiv.org/abs/2303.13450>.
- Eguchi, R. R., Choe, C. A., and Huang, P.-S. Ig-vae: Generative modeling of protein structure by direct 3d coordinate generation. *PLoS computational biology*, 18(6): e1010271, 2022.
- Ferreira, A., Li, J., Pomykala, K. L., Kleesiek, J., Alves, V., and Egger, J. Gan-based generation of realistic 3d data: A systematic review and taxonomy. *arXiv preprint arXiv:2207.01390*, 2022.
- Ha, D. and Schmidhuber, J. Recurrent world models facilitate policy evolution. In *Advances in Neural Information Processing Systems 31*, pp. 2451–2463. Curran Associates, Inc., 2018. <https://worldmodels.github.io>.
- He, Y., Bai, Y., Lin, M., Zhao, W., Hu, Y., Sheng, J., Yi, R., Li, J., and Liu, Y.-J. T³bench: Benchmarking current progress in text-to-3d generation, 2023.
- Kerbl, B., Kopanas, G., Leimkühler, T., and Drettakis, G. 3d gaussian splatting for real-time radiance field rendering. *ACM Transactions on Graphics*, 42(4):139:1–139:14, 2023. doi: 10.1145/3588432.3591417.
- Ko, J., Cho, K., Choi, D., Ryoo, K., and Kim, S. 3d gan inversion with pose optimization. In *Proceedings of the IEEE/CVF Winter Conference on Applications of Computer Vision*, pp. 2967–2976, 2023.
- Kosiorek, A. R., Strathmann, H., Zoran, D., Moreno, P., Schneider, R., Mokrá, S., and Rezende, D. J. Nerf-vae: A geometry aware 3d scene generative model. In *International Conference on Machine Learning*, pp. 5742–5752. PMLR, 2021.
- Kumaran, V., Rowe, J., Mott, B., and Lester, J. Scenecraft: automating interactive narrative scene generation in digital games with large language models. In *Proceedings of the Nineteenth AAAI Conference on Artificial Intelligence and Interactive Digital Entertainment*, AI-IDE ’23. AAAI Press, 2023. ISBN 1-57735-883-X. doi: 10.1609/aiide.v19i1.27504. URL <https://doi.org/10.1609/aiide.v19i1.27504>.
- Lin, C.-H., Gao, J., Tang, L., Takikawa, T., Zeng, X., Huang, X., Kreis, K., Fidler, S., Liu, M.-Y., and Lin, T.-Y. Magic3d: High-resolution text-to-3d content creation. In *Proceedings of the IEEE/CVF Conference on Computer Vision and Pattern Recognition (CVPR)*, pp. 300–309, June 2023.
- Liu, Y., Lin, C., Zeng, Z., Long, X., Liu, L., Komura, T., and Wang, W. Syncdreamer: Generating multiview-consistent images from a single-view image. In *International Conference on Learning Representations (ICLR)*, 2024. Spotlight.
- Ma, B., Deng, H., Zhou, J., Liu, Y.-S., Huang, T., and Wang, X. Geodream: Disentangling 2d and geometric priors for high-fidelity and consistent 3d generation. 2023.
- Metzger, G., Richardson, E., Patashnik, O., Giryes, R., and Cohen-Or, D. Latent-nerf for shape-guided generation of 3d shapes and textures. *arXiv preprint arXiv:2211.07600*, 2022.
- Micheli, V., Alonso, E., and Fleuret, F. Transformers are sample-efficient world models. In *The Eleventh International Conference on Learning Representations*, 2023. URL <https://openreview.net/forum?id=vhFulAcb0xb>.
- Mildenhall, B., Srinivasan, P. P., Tancik, M., Barron, J., Ramamoorthi, R., and Ng, R. Nerf: Representing scenes as neural radiance fields for view synthesis. In *European Conference on Computer Vision (ECCV)*, 2020. URL <https://arxiv.org/abs/2003.08934>.
- Mittal, V. Attngrunder: Talking to cars with attention, 2020. URL <https://arxiv.org/abs/2009.05684>.

- OpenAI. Gpt-4v(ision) system card, 2023. URL <https://openai.com/research/gpt-4>. Version 1.0.
- Petrovich, M., Black, M. J., and Varol, G. Action-conditioned 3d human motion synthesis with transformer vae. In *Proceedings of the IEEE/CVF International Conference on Computer Vision*, pp. 10985–10995, 2021.
- Po, R. and Wetzstein, G. Compositional 3d scene generation using locally conditioned diffusion, 2023. URL <https://arxiv.org/abs/2303.12218>.
- Poole, B., Jain, A., Barron, J. T., and Mildenhall, B. Dreamfusion: Text-to-3d using 2d diffusion. In *International Conference on Learning Representations*, 2023. URL <https://openreview.net/forum?id=FjNys5c7VyY>.
- Qiu, L., Chen, G., Gu, X., Zuo, Q., Xu, M., Wu, Y., Yuan, W., Dong, Z., Bo, L., and Han, X. Richdreamer: A generalizable normal-depth diffusion model for detail richness in text-to-3d. In *Proceedings of the IEEE/CVF Conference on Computer Vision and Pattern Recognition*, pp. 9914–9925, 2024.
- Radford, A., Kim, J. W., Hallacy, C., Ramesh, A., Goh, G., Agarwal, S., Sastry, G., Askell, A., Mishkin, P., Clark, J., Krueger, G., and Sutskever, I. Learning transferable visual models from natural language supervision. *Proceedings of the 38th International Conference on Machine Learning*, 2021. URL <https://arxiv.org/abs/2103.00020>.
- Rombach, R., Blattmann, A., Lorenz, D., Esser, P., and Ommer, B. High-resolution image synthesis with latent diffusion models, 2021.
- Shi, Y., Wang, P., Ye, J., Mai, L., Li, K., and Yang, X. Mvdream: Multi-view diffusion for 3d generation. *arXiv:2308.16512*, 2023.
- Tang, J., Ren, J., Zhou, H., Liu, Z., and Zeng, G. Dream-gaussian: Generative gaussian splatting for efficient 3d content creation. *arXiv preprint arXiv:2309.16653*, 2023.
- Wang, H., Du, X., Li, J., Yeh, R. A., and Shakhnarovich, G. Score jacobian chaining: Lifting pretrained 2d diffusion models for 3d generation. *arXiv preprint arXiv:2212.00774*, 2022.
- Wang, Z., Lu, C., Wang, Y., Bao, F., Li, C., Su, H., and Zhu, J. Prolificdreamer: High-fidelity and diverse text-to-3d generation with variational score distillation. *arXiv preprint arXiv:2305.16213*, 2023.
- Wei, J., Wang, X., Schuurmans, D., Bosma, M., Ichter, B., Xia, F., Chi, E., Le, Q., and Zhou, D. Chain-of-thought prompting elicits reasoning in large language models, 2023. URL <https://arxiv.org/abs/2201.11903>.
- Yang, Y., Sun, F.-Y., Weihs, L., VanderBilt, E., Herrasti, A., Han, W., Wu, J., Haber, N., Krishna, R., Liu, L., Callison-Burch, C., Yatskar, M., Kembhavi, A., and Clark, C. Holodeck: Language guided generation of 3d embodied ai environments, 2024. URL <https://arxiv.org/abs/2312.09067>.
- Zhang, L., Yang, G., and Stadie, B. C. World model as a graph: Learning latent landmarks for planning, 2021.
- Zhao, X., Ma, F., Güera, D., Ren, Z., Schwing, A. G., and Colburn, A. Generative multiplane images: Making a 2d gan 3d-aware. In *European conference on computer vision*, pp. 18–35. Springer, 2022.
- Zhou, X., Ran, X., Xiong, Y., He, J., Lin, Z., Wang, Y., Sun, D., and Yang, M.-H. Gala3d: Towards text-to-3d complex scene generation via layout-guided generative gaussian splatting. *arXiv preprint arXiv:2402.07207*, 2024.
- Zhu, J., Zhuang, P., and Koyejo, S. Hifa: High-fidelity text-to-3d generation with advanced diffusion guidance, 2024. URL <https://arxiv.org/abs/2305.18766>.

A. Appendix

A.1. Implementation details

We select DreamGaussian as the 3D Gaussian generation model, where the guidance scale is set to 100. The learning rates for opacity, position, and color are set to 5×10^{-2} , 1.6×10^{-4} , and 5×10^{-3} , respectively. For texture and mesh extraction of 3D assets, we set the geometry learning rate to 1×10^{-4} and the texture learning rate to 2×10^{-1} , which are used for geometric adjustments of the mesh and enhancing texture details. Regarding the agent design, we use GPT-4 as the core for the natural language analysis and reasoning agents AG-extractor and AG-classifier. For the text-to-2D generation agent AG-generator, DALL-E 3 is used as the core, while for the visual supervision agent AG-supervisor, we select GPT-4o (OpenAI, 2023) for its strong visual understanding capabilities. For capturing scene images used in visual supervision, cameras are placed along each axis, facing the origin, with the distance set to 8. Since our work primarily relies on the designed physical pool and various powerful agents for scene layout, training is not required. High-quality compositional scene generation can be completed in approximately 10 minutes on a 12G NVIDIA 4080 Laptop.

A.2. Physical Relationship Database within the Physical Pool

- Basic relationships: on, under, left, right, front, behind.
- Vague relationships: far, near.
- Alignment relationship: center-aligned.
- Leaning relationship: leaning-on.
- Rotation relationships: facing, rotation.
- Special relationships: duplicate_x_alignment, duplicate_y_alignment, duplicate_facing.

We categorize object relationships into basic, vague, alignment, leaning, and rotational relationships, structuring asset positions in scene descriptions accordingly. To further aid the LLM in understanding overall scene adjustment requirements, we define three special relationships: duplicate_x_alignment refers to “copy and align the entire scene along the x-axis”, duplicate_y_alignment refers to “copy and align the entire scene along the y-axis”, and duplicate_facing refers to “copy and face each other”.

A.3. Primary Agent Prompt

Here, we provide the example of agent prompt engineering, as shown in Figure 5 and Figure 6. We outline the core components of the critical agent prompt engineering process. For AG-extractor, the CoT design encompasses object extraction and image generation, size classification, relationship extraction, special inference, and output example. For AG-supervisor, along with input data configuration and evaluation metrics, it integrates reverse reasoning prompts to enhance its capabilities.

A.4. Agent Reasoning Demonstration

The Figure 7 presents examples of agent reasoning, illustrating the AG-extractor reasoning process for scene graph generation and the AG-supervisor process for scene evaluation and guidance. Leveraging the reflection mechanism mentioned earlier, uncertainty in agent reasoning and generation is significantly reduced, ensuring stable and consistent execution.

A.5. Ground Material Generation

We simulate three types of realistic ground: grass, sandy, and wood ground, using Blender’s asset construction capabilities, as illustrated in Figure 8. First, we determine the ground’s position and materials based on the generated scene. Then, a ground plane is created, followed by the generation of procedural texture nodes, with adjustments to texture density, roughness, and detail levels. Various nodes (such as texture coordinates, mapping, noise, and color gradients) are connected in sequence to produce the desired effect and apply it to the ground. For uneven ground, such as grass, a particle system is added, with particles configured in hair mode to generate grass. Randomness and clustering effects are introduced to control the clumping and roughness of the grass.

You are a master of sentence analysis. Here are some guidelines for you. Note that guidelines are only hints, the Output format follows exactly the Example in the "Output Example":



1. Object Extraction and Image Generation:
Please extract all the objects from the following scene description {set_prompt} and convert them into the format:
"The front image of 'object'. Be simple and complete, with no objects and no decorations, realistic, no shadow, plain white background, light source is directly from above."


2. Object Size Classification:
I have divided the object size into three categories: large, medium, and small. For size classification, the standard is: objects like apples and books are considered small, objects like bikes and chairs are medium, and objects as large as trees and houses are classified as large. Identify the size category of each object and output it in the format:
"object : obj_size"

3. Relationship Inference:
Based on the spatial description {set_prompt}, infer the relationships between the objects according to the following allowed relationships:
- Basic relationships: on, under, left, right, front, behind.
...
- Note that the relationship is only given to the preceding object, the second object is "None". For example, if the input is "a on b and c behind b", then a's relationship is "on", b's relationship is "None", and c's relationship is "behind".

4. special Inference:
From the spatial description {set_prompt}, which copy to make is inferred based on the following allowed copy relations:
- Replication relationships: duplicate_x_alignment, duplicate_y_alignment, duplicate_facing.
The copy relation can only be selected from the above three, and if no copy relation exists, it outputs "None".
...
"Output Example"
--For the input: "A flower near a tree, and an apple on the tree."
**None. The front image of flower, with no objects and no decorations, realistic, without shadow, plain white background, light source is directly from above. flower : large : near.
...

Figure 5. Example of agent AG-extractor prompt.

You are an intelligent scene placement evaluation agent. Evaluate the placement of objects for spatial reasonableness based on coordinates and an image.



Input data:
- Object Coordinates: {coordinates} (example: bike: (0.65, 0.22, 0.07), flower: (0.02, 0.02, 0.01))
- Perspective images (x-direction and -y-direction), the details of the images are under "image_url".
- {grounds} is the z-coordinate of the ground. This ground is the lowest surface obj can step on.
- {turns} is the number of rounds that have taken place so far, start at 0.
...

Evaluation Criteria:
- The coordinates of an object are the coordinates of its geometric center, and all objects are not points, but objects with lengths and widths, which are taken into account when reasoning. You need to roughly estimate the amount of subsequent displacement from the coordinates and view position.
- Focus the assessment on whether an object's location visually violates physical rules (e.g., a bird on a chair should stand on the chair surface, not float above it or on the back). The approximate size and height of similar items in reality can be considered in the reasoning process.
...

Reverse Reasoning Steps:
** Determine the target result **: All objects should be placed properly.
** Identify the problem **: For each object, check if the coordinates meet the evaluation criteria based on the provided description.
- For example, if a bird is at (0.5,0.5,0.1), evaluate whether this position is on the chair seat or somewhere else.
** Adjustment suggestion **: If an object is found to be in an unreasonable position, determine a more suitable position according to the rules of physics. The approximate size and height of similar items in reality can be considered in the reasoning process.
- Here's a proper reasoning:
To adjust the placement of the bird so that it appears to be sitting on the chair, we would need to lower the bird's z-coordinate. Assuming the chair seat is just slightly above the ground, we will consider a reasonable height for a chair seat to be approximately 0.45-0.50 meters off the ground (regular seat height for chairs). From the images, it appears the bird needs to be lowered. We'll tentatively suggest moving the bird down by the difference to a reasonable seat height:
Given the ground z-coordinate is -0.3309211730957031, and assuming the seat is at around 0.45-0.50 meters above the ground, we can estimate the chair seat height to be around 0.12 to 0.17 meters (0.45-0.33 to 0.50-0.33).
...

Figure 6. Example of agent AG-supervisor prompt.

Scene Graph Extraction Reasoning

Scene Description:

A bird is standing on a chair with a frog next to it and Luigi toy is under the chair, A hammer was leaning on the leg of the chair

Scene Graph

[**None. The front image of bird, with no objects and no decorations, realistic, without shadow, plain white background, light source is directly from above. bird : small : on. ', 'The front image of chair, with no objects and no decorations, realistic, without shadow, plain white background, light source is directly from above. chair : medium : None.', 'The front image of frog, with no objects and no decorations, realistic, without shadow, plain white background, light source is directly from above. frog : small : next.', 'The front image of Luigi toy, with no objects and no decorations, realistic, without shadow, plain white background, light source is directly from above. Luigi toy : small : under.', 'The front image of hammer, with no objects and no decorations, realistic, without shadow, plain white background, light source is directly from above. hammer : small : leaning-on. ']

Visual Supervision Reasoning

The output is :

To evaluate the placement of the objects based on their spatial reasonableness, we will consider the provided coordinates, dimensions, and perspective images. Based on the target description of the scene, the expected relationships between the objects are analyzed below:

1. **Bird Placement Evaluation:**

- Current Coordinates: (0.03, 0.07, 0.43)
- Bird Height: 0.13
- Relative to Chair Surface:
 - Chair height (z-coordinate): $0.75/2 = 0.375$ (considering the center to be around this height).
 - The bird's current position suggests that it might be above the seat surface given its height ($0.43 + 0.13/2 > 0.375$).
- Suggested Adjustment:
 - Lower the bird's z-coordinate slightly, since a realistic seating height for a chair can range between 0.45 to 0.50 meters off the ground, corresponding to 0.145 to 0.17 meters on the scene's relative scale (z). Adjust z by about -0.03.

2. **Chair Placement Evaluation:**

- Current Coordinates: (0.00, 0.00, 0.00)
- Chair Dimensions: (0.43, 0.48, 0.75)
- Reasoning:
 - The chair is the foundational object, and given its large dimensions, its placement acts as a reference for other items.
- Suggested Adjustment: None. Its placement is stable and serves as a reference point.

3. **Frog Placement Evaluation:**

- Current Coordinates: (0.00, 0.00, 0.00)
- Frog Height: 0.13
- Reasoning: The frog should be placed next to the bird, around the same surface area on the chair.
- Suggested Adjustment: Slightly adjust coordinates of x and/or y to position next to the bird, but only minimally since specific relative placement is subjective.

4. **Toy Placement Evaluation:**

- Current Coordinates: (0.00, 0.00, -0.26)
- Toy Height: 0.14
- Reasoning: The toy should be under the chair.
- Suggested Adjustment: Ensure the toy's coordinates suggest clearance between the toy and the chair's seat, matching the toy's typical placement beneath a seat.

5. **Hammer Placement Evaluation:**

- Current Coordinates: (-0.26, 0.10, -0.26)
- Hammer Height: 0.14
- Reasoning: The hammer must lean against the chair leg, suggesting its z-coordinate should allow part of it to be supported visibly.
- Suggested Adjustment: Check alignment visually for leaning support.

6. ### Output Summary

...

Figure 7. Example of agent reasoning demonstration.

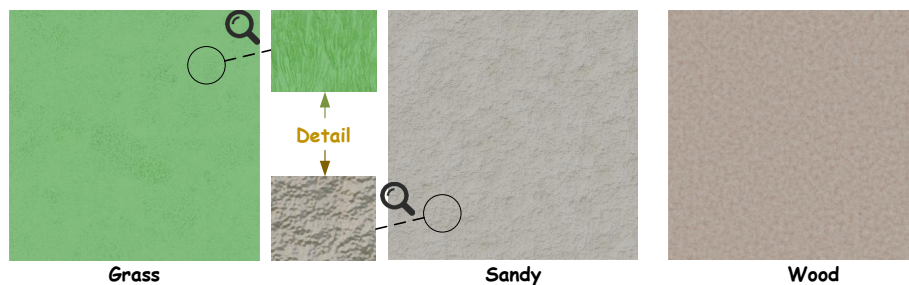


Figure 8. Display of three types of ground.